Solubility-dependent $NiMoO_4$ nanoarchitectures: Direct correlation between rationally designed structure and electrochemical pseudo-kinetics

John Hong[a], Young-Woo Lee[a], Bo Hou[a], Wonbae Ko[b], Juwon Lee[a], Sangyeon Pak[a], JinPyo Hong[b], Stephen M. Morris[a], SeungNam Cha[a,*], Jung Inn Sohn[a,*] and Jong Min Kim[c]

[a] Department of Engineering Science, University of Oxford, Parks Road, Oxford, OX1 3PJ, United Kingdom.

[b] Research Institute of Convergence of Basic Science, Novel Functional Materials and Device Laboratory, Department of Physics, Hanyang University, Seoul 133-791, Korea.

[c] Electrical Engineering Division, Department of Engineering, University of Cambridge, 9 JJ Thomson Avenue, Cambridge, CB3 0FA, United Kingdom.

* Corresponding author. Tel: +44-1865-273912. Fax: +44-1865-273010.

E-mail address: seungnam.cha@eng.ox.ac.uk; junginn.sohn@eng.ox.ac.uk.

Abstract

Pseudocapacitors have recently attracted attention from the scientific community as a promising new energy storage system, which can potentially bridge the performance gap between lithium ion batteries and conventional capacitors. To further improve the performance of these pseudocapacitors, tailoring the binary metal oxide along with developing new methods for controlling resultant nanostructures in a predictive way is an essential requirement for achieving more favorable electrochemical kinetics. Here, through a simple hydrothermal synthetic procedure that uses different supersaturation states to alter the driving force for crystal growth, we have managed to obtain one-dimensional (1-D) Nickel Molybdenum Oxide ($NiMoO_4$) electrodes on a nickel foam. The morphology of the 1-D $NiMoO_4$ nanostructures can be tuned from a low to a high aspect ratio (over a range of diameter sizes from 80 to 800 nm). Such a controllable structure provides a platform for understanding the electrochemical relationships in terms of fast retention times and improved ion diffusion coefficients, enabling the demonstration of promising electrochemical storage properties. We show that the 1-D $NiMoO_4$ electrode with a high aspect ratio (HAR) exhibits a much higher specific capacitance of 1335 F g^{-1} at a current density of 1 A g^{-1}, which is due to the unique physical and chemical structure being suitable for electrochemical kinetics. We further demonstrate that an asymmetric supercapacitor consisting of the tailored HAR-$NiMoO_4$ electrode can achieve an energy density of 40.7 Wh kg^{-1} and a power density of 16 kW kg^{-1}.

Keywords: Energy storage material, Electrochemical reaction kinetics, Nanowire architecture, Controlled aspect ratio, Asymmetric supercapacitor

1. INTRODUCTION

Electrochemical supercapacitors are currently being considered as promising candidates for next-generation energy storage applications since they have the potential to bridge the gap between batteries and conventional capacitors for the production of high power and high energy densities. Furthermore, they have been shown to exhibit a good rate capability, long cycling life time, and environmentally friendly characteristics.[1-3] In particular, pseudocapacitors, which possess the capability to store large amounts of charge *via* fast and reversible electrochemical Faradaic redox reactions, have enormous potential in a broad variety of applications, including electric vehicles and portable electronic devices.[4,5] Currently, transition metal oxides/hydroxides such as RuO_2, $Ni(OH)_2$, Co_3O_4 and MnO_2, are most commonly used as the electrode materials with high theoretical capacitances because of their multiple oxidation states, enabling rich electrochemical Faradaic reactions.[6-9]

Despite their compelling benefits combined with the inherently high electrochemical activities, their low conductivity and structural instability, which leads to a reduction in the performance, continuously hinders the successful exploitation of pseudocapacitor technology in practical applications.[10] To overcome these limitations, numerous studies have been devoted to enhancing the electrochemical properties of the pseudocapacitors by focusing on the development of new electrode materials that are based on binary transition metal oxides.[11-14] These materials typically exhibit a higher electrical conductivity and richer chemical valence states than the single-component transition metal oxides, which arises from the combined contributions from both metal atoms.[11-14] Among the various binary metal oxides, transition metal molybdates such as $NiMoO_4$ and $CoMoO_4$ are an emerging class of pseudocapacitor materials that have received considerable attention due to their cost-effectiveness, abundance, and chemical stability.[15,16] More specifically, the primary interest in $NiMoO_4$ lies in the fact that the high specific capacitance from the Ni atom and the high electrical conductivity from the Mo atom can contribute collectively to the superior electrochemical behavior when used in energy storage devices.[17] Combined, these features demonstrate that $NiMoO_4$ has potential in future pseudocapacitor energy storage systems.

Alternatively, various nanostructuring approaches have been developed to address issues related to limited electrochemical kinetics on the surface, which are strongly associated with a low degree of surface contact areas and low ion diffusion rates.[18-19] These more recent strategies have shown that hierarchical nanostructures with diverse morphologies and dimensions (D) can provide more active sites and shorter ion diffusion pathways, which then stimulate and facilitate the kinetics associated with the electrochemical reactions. In particular, 1-D nanostructures are one of the most widely used architectures for electrochemical storage devices mainly because 1) the unique geometry results in a large contact surface area; 2) the structures exhibit short diffusion distance; 3) they exhibit good structural stability and 4) they possess a favorable charge carrier path during the charge/discharge processes. Nevertheless, synthesizing these 1-D structures in binary metal oxides in a controlled way still remains a challenge and is mainly due to the complex stoichiometry-dependent synthetic reactions. Further, even though there have been few reports[20-21] that have studied the dependence of the electrochemical storage performance on the different nanostructures, there are no detailed studies that directly describe the electrochemical ion intercalation mechanism for engineering 1-D nanostructures with tailored aspect ratios.

It is, therefore, highly desirable that a novel and facile synthetic route for the preparation of 1-D nanostructured binary metal oxides with different aspect ratios be developed that can enhance the charge transfer kinetics so as to improve charge transportation. Moreover, developing such a procedure would enable us to understand how the charge storage dynamics and electrochemical stability depends upon the nanostructure and how this can lead to a superior pseudocapacitor performance. To this end, we have employed the fundamental principle of hydrothermal reaction kinetics whereby the nucleation and crystallization growth rates can depend crucially on the supersaturation states of the solvents, which are the major driving forces for solution-based synthetic processes as shown in Figures 1a-c.[22] Controlling the rational supersaturated environments enables the synthesis of 1-D $NiMoO_4$ nanostructures with different, but predictable, morphologies. In this regard, we propose a simple and facile way for the rational and precise design of the desirable supersaturation levels, which in turn affects the crystal nucleation rates and preferred crystal growth geometries and directions thereby leading to different 1-D aspect ratios. Moreover, the different 1-D $NiMoO_4$ nanostructures can result in a diverse range of electrochemical behavior including specific capacitance as well as ion diffusion and charge transfer dynamics. Through the control of these properties, it therefore provides one of the best routes for the design of new electrode materials for high-performance supercapacitors.

2. EXPERIMENTAL DETAILS

2.1 Material synthesis: $NiMoO_4$ nanostructures on a Ni foam.

Different 1-D $NiMoO_4$ nanostructures with different aspect ratios on nickel foams were synthesized by a hydrothermal method. First, a conductive Ni foam (1 cm x 1 cm) was cleaned using 1 M HCl, ethanol, and deionized water. In a typical synthesis, 1.0 mmol of $Ni(NO_3)_2 \cdot 6H_2O$ and 1.0 mmol of Na_2MoO_4 were dissolved in deionized water at room temperature to form a clear green solution. After being stirred for an hour, the solution was transferred into a 45 ml Teflon-lined cup, and then the Ni foam was transferred into the Teflon-lined cup and a stainless steel autoclave. The hydrothermal reaction was carried out at 140 ^{o}C for 4 hr. After cooling down naturally to room temperature, the Ni foam was collected and washed several times with water and ethanol to remove loosely attached $NiMoO_4$ on the

Ni foam. The foam was then fully dried at 60 ^{o}C for 12 hr. In order to obtain the crystallized $NiMoO_4$ nanostructures, the Ni foam with the $NiMoO_4$ nanostructure was calcined at 400 ^{o}C for 2 hr in an argon atmosphere. The different nanostructures of the $NiMoO_4$ material were synthesized using various solvents with different mixtures of solvents such as water, ethanol and hydrochloric acids.

2.2 Material characterization

Morphologies of the samples were characterized by SEM (Hitachi S-4300) and TEM (JEOL JEM-2200MCO FEGTEM). The crystal structure of the samples was examined by high resolution XRD (Rigaku Medel Smartlab) in a two theta range of 10-80º. The specific BET surface area was calculated on the basis of nitrogen adsorption isotherms using Micromeritics Gemini VI. XPS were recorded using a Thermo Scientific K-Alpha XPS instrument equipped with a micro-focused mono-chromated Al X-ray source. The XPS source was operated at 12 keV and a 400 μm spot size was used. The spectrometer was adjusted to align a binding energy of 284.5eV for the C 1s line.

2.3 Electrochemical characterization

The electrochemical properties of the $NiMoO_4$ samples with different aspect ratios were measured in a three-electrode system consisting of HAR-, MAR-, and LAR-$NiMoO_4$ electrodes as working electrodes, Pt mesh as a counter electrode, and an Ag/AgCl electrode (in saturated 3 M KCl) as a reference electrode. These were used to analyze CV, galvanostatic charge/discharge, and EIS curves using a potentiostat (PGSTAT302N, Metrohm, Autolab). For the fabrication of the anode electrodes, active carbon was prepared as an active material, with poly(vinylidene difluoride) as a binder and Ketjen black as a conductive material, and this was then coated onto the compressed nickel foam as a current collector. All electrochemical results of the AC//HAR-$NiMoO_4$ ASC were measured using a two electrode system under 1.0 M KOH solution at room temperature.

3. RESULTS AND DISCUSSION

The morphology and structural characteristics of the as-prepared $NiMoO_4$ materials were investigated by scanning electron microscopy (SEM). As shown in Figures 1d-f, the controlled growth of the 1-D $NiMoO_4$ nanostructures with different aspect ratios was successfully achieved on a nickel foam through a hydrothermal process by adjusting the solubility level in the reaction solution and hence introducing various different supersaturation states during the growth phase. Obviously, as the relative solubility decreases, the morphology of the 1-D nanostructures is transformed through a series of distinct aspect ratios between length to breadth from a low (LAR) to a high value (HAR) through a medium value (MAR). Figure 1d shows an SEM image of the MAR-$NiMoO_4$ sample obtained from the DI water-only solution, which results in 1-D nanostructures with a diameter size of ~250 nm. In contrast, the HAR-$NiMoO_4$ sample with a diameter of about 80 nm is grown under low solubility conditions induced by adding an alkaline solvent into the water solution (Figure 1d). Finally, the LAR-$NiMoO_4$ sample has a diameter of 800 nm and was constructed by introducing an additional acidic solvent (Figure 1f). These findings indicate that introducing a low (high) solubility environment to the hydrothermal precursor solution induces the relatively high (low) degree of supersaturation, leading to a higher (lower) driving force for crystal nucleation and growth process. Therefore, the selective synthesis mechanism responsible for the different 1-D $NiMoO_4$ structures can be understood in terms of the control of the solvent solubility that leads to different degrees of supersaturation. Moreover, a predictable 1-D nanostructure synthetic route so as to grow the active materials directly on to a metal collector means that the driving force for nucleation and crystal growth can be controlled by changing the supersaturation states.

Next, the nanostructures of the HAR-, MAR- and LAR-$NiMoO_4$ samples were further characterized by transmission electron microscopy (TEM) to provide more insight regarding their unique 1-D structure, as shown in inset images of Figures 1d-f. The TEM images clearly demonstrate that the diameter of 1-D nanostructures for the as-prepared $NiMoO_4$ samples is in good agreement with the SEM results. As a result of tuning the solubility of the solvents, three different types of 1-D $NiMoO_4$ material with mean aspect ratios of 21.6 (HAR-$NiMoO_4$), 12.8 (MAR-$NiMoO_4$), and 4.7 (LAR-$NiMoO_4$) were successfully prepared for use in a supercapacitor application (Supporting Information Figure S1).

To evaluate the crystallographic phase of the $NiMoO_4$ electrode samples, X-ray diffraction (XRD) spectra were analyzed, which are shown in Figure 2a. All the diffraction patterns obtained from the 1-D $NiMoO_4$ nanostructures with different aspect ratios are unambiguously assigned to the $NiMoO_4$ phase (JCPDS Card No. 86-0361) without any noticeable differences.[23] Moreover, to confirm the surface electronic states and chemical compositions of the $NiMoO_4$ samples, X-ray photoelectron spectroscopy (XPS) measurements were carried out. Figures 2c-d compare the high resolution XPS spectra of the Ni 2p and Mo 3d of the 1-D $NiMoO_4$ samples with different aspect ratios, respectively. The Ni 2p doublet is clearly observed at 854.9 eV (Ni^{2+} $2p_{3/2}$) and at 872.5 eV (Ni^{2+} $2p_{1/2}$) with a p spin-orbit splitting of 17.6 eV.[24] Moreover, the two peaks at binding energies of 232.0 eV and 235.1 eV with the d spin-orbit splitting of 3.1 eV correspond to Mo^{6+} $3d_{5/2}$ and Mo^{6+} $3d_{3/2}$, respectively.[25] These XPS results suggest that there are only chemical oxidation states and compositions of the Ni^{2+} and Mo^{6+} in the as-prepared 1-D $NiMoO_4$ whereby the Ni cations, distributed in octahedral sites, are electrochemically active with OH^- electrolyte ions and the Mo cations in tetrahedral sites contribute to the electrochemical stability.

To further examine the specific surface area characteristics of the 1-D $NiMoO_4$ structures, measurements of the N_2 adsorption-desorption were carried out (Supporting

Information Figure S2). As shown in Figure 2b, the calculated Brunauer-Emmett-Teller (BET) surface area of the HAR-$NiMoO_4$ sample has the largest value (97.26 m^2 g^{-1}) and is much larger than the areas for the MAR-$NiMoO_4$ (50.32 m^2 g^{-1}) and LAR-$NiMoO_4$ (25.66 m^2 g^{-1}) samples, which is mainly due to the different aspect ratios of the nanostructures. This implies that the high surface area of the HAR-$NiMoO_4$ electrodes provides a sufficient electrolyte contact interface and can thus enhance the kinetics of ion diffusion. Consequently, a high aspect ratio can improve the electrochemical capacitance and the charge transfer kinetics.

In order to evaluate the electrochemical performance of the different 1-D morphologies, the HAR-, MAR- and LAR-$NiMoO_4$ were applied directly as working electrodes in a three electrode system. Supporting Information Figure S3 shows the cyclic voltammetry (CV) and the galvanostatic charge-discharge curves of the each $NiMoO_4$ electrode. First, the CV curves of all the $NiMoO_4$ electrodes have similar shapes with increasing scan rates, indicating that all the electrodes have good pseudocapacitive behavior.[26] For a direct CV performance comparison between the electrodes, Figure 3a presents the CV curves of the three different types of $NiMoO_4$ electrodes with the potential window ranging from 0.0 to 0.6 V at a scan rate of 5 mV s^{-1}. It can be clearly observed that all the $NiMoO_4$ electrodes have a couple of Faradaic reaction peaks that can be ascribed to the reversible redox reaction between Ni(II) and Ni(III).[27] The area surrounded within the CV curve of the HAR-$NiMoO_4$ sample occupies the largest area, indicating the highest value for the electrochemical capacitance. This large CV area might be attributed to the larger electrolyte contact area for the HAR-$NiMoO_4$ electrode. Consistent with the CV results, the galvanostatic charge-discharge curves demonstrate that the HAR-$NiMoO_4$ electrode has the longest discharge time (Supporting Information Figure S3). Moreover, the calculated specific capacitance of the HAR-, MAR-, and LAR-$NiMoO_4$ samples at a current density of 1 A g^{-1}

are 1335 F g^{-1}, 1106 F g^{-1} and 672 F g^{-1}, respectively (Supporting Information Figure S4).

In order to better understand the ion diffusion behavior and charge transfer dynamics of the $NiMoO_4$ electrodes with tailored aspect ratios, kinetic electrochemical analysis was carried out. The inset of Figure 3a indicates the potential difference of each electrode between the anodic and cathodic peak, representing the degree of reversible intercalation and de-intercalation dynamics during the CV charge-discharge.[28] It can be seen that the HAR-$NiMoO_4$ electrode provides a much more appreciable OH^- ion access and faster charge transfer rate. Moreover, the cathodic peak current densities of the $NiMoO_4$ electrodes were plotted as a function of the square root of the scan rates in Figure 3b. The cathodic peak currents increase linearly, showing that redox reactions at the surface are followed by a diffusion-controlled process with the OH^- ions.[29] Also, it is evident that the cathodic peak current of the HAR-$NiMoO_4$ sample shows a steeper dependence compared to the other electrodes, indicating a larger diffusion coefficient. For a direct comparison of the ion diffusivity, the diffusion coefficients of the $NiMoO_4$ electrodes were calculated according to the following Randles–Sevcik equation.[30]

$$\mathrm{i_p} = (2.69 * 10^5) * n^{\frac{3}{2}} * A * D_0^{\frac{1}{2}} * C_0 * \upsilon^{\frac{1}{2}}$$

where i_p is the cathodic peak current density, n is the number of electrons, A is the electrode area, D_0 is the diffusion coefficient, C_0 is the electrolyte concentration, and υ is the scan rate. We can assume that n, A, C_0 have the same values in the same three electrode system. Therefore, the diffusion coefficient of the 1-D $NiMoO_4$ samples can be directly compared from the slope of the curve ($D_0^{\frac{1}{2}} \propto i_p/\upsilon^{\frac{1}{2}}$) . The diffusion coefficient of the HAR-NiMoO4 sample is found to be 1.82 and 17.9 times larger than that of the MAR- and LAR-NiMoO4 samples, respectively.

Figure 3c presents the specific rate retention data as a function of the current density in the electrodes. From a low current density of 1 A g^{-1} to a high current density of 20 A g^{-1}, the capacitance of the HAR-$NiMoO_4$ electrode shows good rate retention behavior, which is found to be 882.4 F g^{-1} at 20 A g^{-1} with ~ 66.1 % retention compared to that for 1 A g^{-1}. On the other hand, for the MAR and LAR-$NiMoO_4$ electrodes the capacitance is recorded to be 668.8 F g^{-1} and 146.0 F g^{-1} with 60.5 % and 21.8 % rate retention, respectively. In other words, the presence of the fast diffusion rate from the surface to the internal structure means that the HAR-$NiMoO_4$ electrode exhibits much better retention performance.

Finally, to elucidate further the ion diffusion and charge transfer behavior, electrochemical impedance spectroscopy (EIS) measurements with Bode phase plots and Nyquist plots were conducted and plotted, respectively (Figure 3d and Supporting Information Figures S5). All the Nyquist plots for the $NiMoO_4$ electrodes show that the charge transfer resistances (R_{ct}), recorded from the diameters of the semicircle, are very low. This outcome demonstrates that the $NiMoO_4$ electrodes grown directly on the Ni foam current collector have nearly equal electrolyte resistance and superior charge transfer, which minimizes interfacial resistant and facilitates charge transfer at the interface between the current collector and electrode material. Furthermore, the linear part in the plot of the HAR-$NiMoO_4$ sample in the low frequency region (Warburg impedance) is significantly steeper than that for the MAR- and LAR-$NiMoO_4$ samples, suggesting that the HAR-$NiMoO_4$ has the fastest ion diffusion and electrolyte access to the surface, which is consistent with the results of the capacitance rate retention in Figure 3c.[31]

Figure 3d shows the Bode phase plots for the $NiMoO_4$ electrodes with the different relaxation time constant (τ_0). A relaxation time constant can be calculated from the x-axis frequency when the curve reaches -45˚ on the Bode plot. The relaxation time constant is an important parameter so as to compare between capacitive and resistive behaviors of a supercapacitors dependence on frequency.[32] As shown in Figure 3d, the HAR-$NiMoO_4$

sample exhibits the fastest relaxation time constant (τ_0 = 1.73 s) compared to that of the MAR- and LAR-$NiMoO_4$ samples which are 3.49 s and 6.87 s, respectively. Here, it should be noted that the fast relaxation time constant implies that the HAR-$NiMoO_4$ sample can introduce a fast capacitive response. It can be clearly observed that the phase angle of HAR-$NiMoO_4$ at a low frequency of f = 0.01 Hz was about -81˚, which is the closest value to -90˚, implying ideal capacitor behavior because of its low electrolyte resistance and fast electrolyte intercalation.[33] Overall, the electrochemical relationships for the $NiMoO_4$ electrodes with the different 1-D morphologies are illustrated in Figure 3e. The HAR-$NiMoO_4$ electrode nanostructure not only provides the largest contact sites, which lead to a large density of electrolyte ions near the surface, but also facilitates more efficient electrochemical reactions through the highest degree of ion diffusion towards the inside of the electrode. Additionally, its high electrical conductivity and low surface resistance enable fast charge transfer through a pseudocapacitor system. Such behavior is strongly correlated to the high capacitance, fast retention rate and charge transfer mechanism of the HAR-$NiMoO_4$ electrode.

To further demonstrate the potential of the $NiMoO_4$ electrode for practical supercapacitor applications, an asymmetric supercapacitor (ASC) was fabricated using the HAR-$NiMoO_4$ material as the cathode and active carbon (AC) as the anode. Figure 4a shows the comparative CV plots of the individual positive and negative electrodes in the ASC at a scan rate of 5 mV s^{-1}. The AC exhibits a typical rectangular electric double-layer capacitor (EDLC) performance within the range of -1.0 to 0.0 V, and the HAR-$NiMoO_4$ shows pseudocapacitance behavior within the range of 0.0 to 0.6 V. Therefore, the AC//HAR-$NiMoO_4$ ASC can operate from 0 to 1.6 V with a wide operating potential. To design the ASC with the ideal capacitance, the mass of the individual electrodes is optimized according to the following formula.[34]

$$Q_{+} = Q_{-} \rightarrow \frac{m_{+}}{m_{-}} = \frac{C_{-} * \Delta V_{-}}{C_{+} * \Delta V_{+}}$$

where C_{-} and C_{+} are the calculated capacitance of the negative and positive electrodes, respectively, and ΔV_{-} and ΔV_{+} are the operating potential windows of the negative and positive electrodes, respectively. Therefore, on the basis of C_{-} and the potential window of the AC electrode, the optimum loading ratio of HAR-$NiMoO_4$ to AC is 1:3.126.

Figure 4b shows CV curves of the ASC device at various scan rates, ranging from 50 to 5 mV s^{-1}. It can be seen that the shape of the CV curves involves both EDLC and pseudocapacitance contribution from the rectangular shape and the redox humps. The CV curves of the ASC are found to maintain a similar profile with increasing scan rates, indicating good capacitive behavior. As shown in the inset of Figure 4c, galvanostatic charge/discharge curves for the ASC were measured at current densities from 1 to 20 A g^{-1} in a potential window of 0 to 1.6 V. In addition, the calculated capacitance as a function of the discharge current density is plotted (Supporting Information Figure S4). This device shows good electrochemical performance and the specific capacitance was calculated to be 114.4 F g^{-1} at a current density of 1 A g^{-1}. Furthermore, the ASC exhibits good cycling stability, retaining up to 82.2 % after 2000 charge-discharge cycles at a current density of 5 A g^{-1} (Figure 4c). To compare the energy density and power density with other reported ASCs, the Ragone plots of the AC//HAR-$NiMoO_4$ ASC were derived in Figure 4d, showing that an energy density of 40.6 Wh kg^{-1} and a power density of 16 kW kg^{-1} can be achieved. Clearly, the device performance compares favorably with other asymmetric supercapacitors.[35-41] It is shown that the HAR-$NiMoO_4$ exhibits a high specific capacitance and high ionic and electric transfer rates, along with good electrochemical behavior because: (1) the direct growth of the 1-D $NiMoO_4$ sample on the Ni foam provides good electron transfer due to the low contact resistance between the active material and the current collector; (2) the highly ordered 1-D nanostructure with a high aspect ratio not only leads to a large diffusion coefficient, but also results in a large contact area and (3) this gives rises to numerous ion diffusion channels, thereby inducing a high rate retention response.

CONCLUSION

In summary, we have demonstrated that 1-D $NiMoO_4$ electrodes grown directly onto a nickel foam have been successfully prepared via a simple supersaturation-controlled hydrothermal process. The resulting 1-D $NiMoO_4$ electrodes, each with a different aspect ratio, can be predictively adjusted by changing the supersaturation states and consequently the driving force for nucleation and crystal growth. Moreover, electrochemical measurements indicate that the HAR-$NiMoO_4$ electrode exhibits the best specific capacitance and superior rate retention performance such as a large specific capacitance of 1335 F g^{-1} at a current density of 1 A g^{-1} with a good rate retention of 66.1 %. We also showed that the AC//HAR-$NiMoO_4$ ASC with a wide potential window of 1.6 V exhibits the energy density of 40.7 Wh kg^{-1} and the power density of 16 kW kg^{-1} compared to other reported pseudo-capacitive ASCs. Furthermore, we successfully demonstrated that the HAR-$NiMoO_4$ electrode provides a better contact surface area, ion diffusion behavior and enhanced charge transfer kinetics based on the hierarchical 1-D nanostructure. This deterministic and predictive synthesis method, which is controlled by adjusting the solubility in a hydrothermal approach, is a promising technique to producing highly efficient pseudo-capacitive electrodes with 1-D nanostructures. Such electrodes can easily promote dynamic electrochemical kinetics, including high Faradaic capacitance, high retention and fast charge transfer rate for practical pseudocapacitor applications.

Acknowledgments

This work was supported by the Industrial Fundamental Technology Development Program from the Ministry of Trade, Industry and Energy (MOTIE) of Korea [10052745, Development of nano-sized (100nm) manganese ceramic material for high voltage pseudo-capacitor]; International Collaborative Energy Technology R&D Program of the Korea Institute of Energy Technology Evaluation and Planning (KETEP) from Ministry of Trade, Industry & Energy of Korea [20138520030800]. Also, SMM acknowledges The Royal Society for financial support.

Figure captions

Figure 1. Illustration of the nanostructures and crystal growth mechanisms of (a) HAR-, (b) MAR- and (c) LAR-$NiMoO_4$ 1-D nanostructures with different aspect ratios. 1-D nanostructures are systematically controlled by using different supersaturation states during the growth phase. (d-f) SEM images of the HAR-, MAR- and LAR-$NiMoO_4$ 1-D nanostructures. Inset images show the corresponding TEM images of the three different 1-D nanostructures.

Figure 2. (a) XRD patterns of the as-prepared $NiMoO_4$ nanostructures. Asterisks show XRD patterns of the nickel foam. (b) Calculated BET specific surface areas of the as-prepared $NiMoO_4$ nanostructures. (c) Ni 2p and (d) Mo 3d XPS spectra of the as-prepared $NiMoO_4$ nanostructures. Inset: images show that Ni cations in the octahedral site and Mo cations in the tetrahedral site contribute to the electrochemical reaction and stability, respectively.

Figure 3. (a) CV curves for HAR-, MAR-, and LAR-$NiMoO_4$ electrodes at a scan rate of 5 mV s^{-1} in 1.0 M KOH. The inset shows the redox potential gap (ΔE_p) for the different $NiMoO_4$ samples. (b) Cathodic peak current density as a function of the square root of the scan rate for the three different samples. (c) Comparison of the capacitance retention and (d) Bode phase plots for the HAR-, MAR-, and LAR-$NiMoO_4$ samples. (e) Illustration of the relationship between the tailored $NiMoO_4$ nanostructures and the pseudo-capacitive behavior including electrolyte ion diffusion and electron transfer dynamics.

Figure 4. (a) Comparative CV curves of the HAR-$NiMoO_4$ and AC electrodes at 5 mV s^{-1} in a three electrode system. (b) CV curves and (c) Cycling stability of the AC//HAR-$NiMoO_4$ ASC. The inset image shows galvanostatic charge-discharge curves of the ASC. (d) Ragone plot of the AC//HAR-$NiMoO_4$ ASC in comparison with other reported ASCs.

References

1 Wang, G.; Zhang, L.; Zhang, J. A Review of Electrode Materials for Electrochemical Supercapacitors. *Chem. Soc. Rev.* **2011**, *41*, 797–828.

2 Yan, J.; Wang, Q.; Wei, T.; Fan, Z. Recent Advances in Design and Fabrication of Electrochemical Supercapacitors with High Energy Densities. *Adv. Energy Mater.* **2014**, *4*, 1300816.

3 Simon, P.; Gogotsi, Y. Materials for Electrochemical Capacitors. *Nature Mater.* **2008**, *7*, 845–854.

4 Augustyn, V.; Simon, P.; Dunn, B. Pseudocapacitive Oxide Materials for High-Rate Electrochemical Energy Storage. *Energy Environ. Sci.* **2014**, *7*, 1597–1614.

5 Fisher, R.; Watt, M.; Ready, W. Functionalized Carbon Nanotube Supercapacitor Electrodes: A Review on Pseudocapacitive Materials. *ECS J. Solid State Sci. Technol.* **2013**, *2*, M3170–M3177.

6 Chou, J.-C.; Chen, Y.-L.; Yang, M.-H.; Chen, Y.-Z.; Lai, C.-C.; Chiu, H.-T.; Lee, C.-Y.; Chueh, Y.-L.; Gan, J.-Y. RuO_2/MnO_2 Core–shell Nanorods for Supercapacitors. *J. Mater. Chem. A* **2013**, *1*, 8753–8758.

7 Zhu, Y.; Cao, C.; Tao, S.; Chu, W.; Wu, Z.; Li, Y. Ultrathin Nickel Hydroxide and Oxide Nanosheets: Synthesis, Characterizations and Excellent Supercapacitor Performances. *Sci. Rep.* **2014**, *4*, 5787.

8 Liu, W.; Li, X.; Zhu, M.; He, X. High-Performance All-Solid State Asymmetric Supercapacitor Based on Co_3O_4 Nanowires and Carbon Aerogel. *J. Power Sources* **2015**, *282*, 179–186.

9 Ma, X.; Kolla, P.; Zhao, Y.; Smirnova, A.; Fong, H. Electrospun Lignin-Derived Carbon Nanofiber Mats Surface-Decorated with MnO_2 Nanowhiskers as Binder-Free Supercapacitor Electrodes with High Performance. *J. Power Sources* **2016**, *325*, 541–

548.

10 Wu, Z.; Zhu, Y.; Ji, X. $NiCo_2O_4$-Based Materials for Electrochemical Supercapacitors. *J. Mater. Chem. A* **2014**, *2*, 14759–14772.

11 Li, L.; Peng, S.; Cheah, Y.; Teh, P.; Wang, J.; Wee, G.; Ko, Y.; Wong, C.; Srinivasan, M. Electrospun Porous $NiCo_2O_4$ Nanotubes as Advanced Electrodes for Electrochemical Capacitors. *Chem. - A Euro. J.* **2013**, *19*, 5892–5898.

12 Hu, J.; Li, M.; Lv, F.; Yang, M.; Tao, P.; Tang, Y.; Liu, H.; Lu, Z. Heterogeneous $NiCo_2O_4$@polypyrrole Core/sheath Nanowire Arrays on Ni Foam for High Performance Supercapacitors. *J. Power Sources* **2015**, *294*, 120–127.

13 Pendashteh, A.; Rahmanifar, M.; Kaner, R.; Mousavi, M. Facile Synthesis of Nanostructured $CuCo_2O_4$ as a Novel Electrode Material for High-Rate Supercapacitors. *Chem. Comm.* **2013**, *50*, 1972–1975.

14 Peng, S.; Li, L.; Hu, Y.; Srinivasan, M.; Cheng, F.; Chen, J.; Ramakrishna, S. Fabrication of Spinel One-Dimensional Architectures by Single-Spinneret Electrospinning for Energy Storage Applications. *ACS Nano* **2015**, *9*, 1945–1954.

15 Li, L.; Peng, S.; Wu, H.; Yu, L.; Madhavi, S.; Lou, X. A Flexible Quasi-Solid-State Asymmetric Electrochemical Capacitor Based on Hierarchical Porous V_2O_5 Nanosheets on Carbon Nanofibers. *Adv. Energy Mater.* **2015**, *5*, 1500753.

16 Xia, X.; Lei, W.; Hao, Q.; Wang, W.; Wang, X. One-Step Synthesis of $CoMoO_4$/graphene Composites with Enhanced Electrochemical Properties for Supercapacitors. *Electrochim. Acta* **2013**, *99*, 253–261.

17 Xiao, K.; Xia, L.; Liu, G.; Wang, S.; Ding, L.-X.; Wang, H. Honeycomb-like $NiMoO_4$ Ultrathin Nanosheet Arrays for High-Performance Electrochemical Energy Storage. *J. Mater. Chem*. A **2015**. *3*, 6128-6135.

18 Wang, S.; Sun, S.; Li, S.; Gong, F.; Li, Y.; Wu, Q.; Song, P.; Fang, S.; Wang, P. Time

and Temperature Dependent Multiple Hierarchical $NiCo_2O_4$ for High-Performance Supercapacitors. *Dalton Tran.* **2016**, *45*, 7469–7475.

19 Zhang, G.; Lou, X. Controlled Growth of $NiCo_2O_4$ Nanorods and Ultrathin Nanosheets on Carbon Nanofibers for High-Performance Supercapacitors. *Sci Rep.* **2013**, *3*, 1470.

20 Xiang, N.; Ni, Y.; Ma, X. Shape-Controlled Synthesis of $NiCo_2O_4$ Microstructures and Their Application in Supercapacitors. *Chem. Asian J.* **2015**, *10*, 1972–1978.

21 Zhu, T.; Koo, E.; Ho, G. Shaped-Controlled Synthesis of Porous $NiCo_2O_4$ with 1-3 Dimensional Hierarchical Nanostructures for High-Performance Supercapacitors. *RSC Adv.* **2014**, *5*, 1697–1704.

22 Chithambararaj; Yogamalar, R.; Bose, C. Hydrothermally Synthesized H-MoO_3 and A-MoO_3 Nanocrystals: New Findings on Crystal-Structure-Dependent Charge Transport. *Cryst. Growth. Des.* **2016**, *16*, 1984–1995.

23 Huang, Z.; Zhang, Z.; Qi, X.; Ren, X.; Xu, G.; Wan, P.; Sun, X.; Zhang, H. Wall-like Hierarchical Metal Oxide Nanosheet Arrays Grown on Carbon Cloth for Excellent Supercapacitor Electrodes. *Nanoscale* **2016**, *8*, 13273–13279.

24 Yan, J.; Fan, Z.; Sun, W.; Ning, G.; Wei, T.; Zhang, Q.; Zhang, R.; Zhi, L.; Wei, F. Advanced Asymmetric Supercapacitors Based on $Ni(OH)_2$/Graphene and Porous Graphene Electrodes with High Energy Density. *Adv. Funct. Mater.* **2012**, *22*, 2632–2641.

25 Ghosh, D.; Giri, S.; Das, C. Synthesis, Characterization and Electrochemical Performance of Graphene Decorated with 1D $NiMoO_4{\cdot}nH_2O$ Nanorods. *Nanoscale* **2013**, *5*, 10428–10437.

26 Pang, H.; Wei, C.; Li, X.; Li, G.; Ma, Y.; Li, S.; Chen, J.; Zhang, J. Microwave-Assisted Synthesis of NiS_2 Nanostructures for Supercapacitors and Cocatalytic Enhancing Photocatalytic H_2 Production. *Sci. Rep.* **2014**, *4*, 3577.

27 Senthilkumar, B.; Sankar, K.; Selvan, R.; Danielle, M.; Manickam, M. Nano A-$NiMoO_4$ as a New Electrode for Electrochemical Supercapacitors. *RSC Adv.* **2012**, *3*, 352–357.

28 Mai, L.; Li, H.; Zhao, Y.; Xu, L.; Xu, X.; Luo, Y.; Zhang, Z.; Ke, W.; Niu, C.; Zhang, Q. Fast Ionic Diffusion-Enabled Nanoflake Electrode by Spontaneous Electrochemical Pre-Intercalation for High-Performance Supercapacitor. *Sci. Rep.* **2013**, *3*, 1718.

29 Xu, P.; Liu, J.; Yan, P.; Miao, C.; Ye, K.; Cheng, K.; Yin, J.; Cao, D.; Li, K.; Wang, G. Preparation of Porous Cadmium Sulphide on Nickel Foam: A Novel Electrode Material with Excellent Supercapacitor Performance. *J. Mater. Chem. A* **2016**, *4*, 4920–4928.

30 Liu, S.; Hui; Hui Flower-like Copper Cobaltite Nanosheets on Graphite Paper as High-Performance Supercapacitor Electrodes and Enzymeless Glucose Sensors. *ACS Appl. Mater. Interfaces* **2016**, *8*, 3258–3267.

31 Pendashteh, A.; Moosavifard, S.; Rahmanifar, M.; Wang, Y.; El-Kady, M.; Kaner, R.; Mousavi, M. Highly Ordered Mesoporous $CuCo_2O_4$ Nanowires, a Promising Solution for High-Performance Supercapacitors. *Chem. Mater.* **2015**, *27*, 3919–3926.

32 Pan, X.; Ren, G.; Hoque, M. N. F.; Bayne S.; Zhu, K.; Fan, Z. Fast Supercapacitors Based on Graphene-Bridged V_2O_3/VO_x Core–Shell Nanostructure Electrodes with a Power Density of 1 MW kg^{-1}. *Adv. Mater. Inter.* **2014,** *1*, 1400398.

33 Yuan, L.; Lu, X.-H.; Xiao, X.; Zhai, T.; Dai, J.; Zhang, F.; Hu, B.; Wang, X.; Gong, L.; Chen, J.; Hu, C.; Tong, Y.; Zhou, J.; Wang, Z. L. Flexible Solid-State Supercapacitors Based on Carbon Nanoparticles/MnO_2 Nanorods Hybrid Structure. *ACS Nano* **2012**, *6*, 656–661.

34 Ren, X.; Guo, C.; Xu, L.; Li, T.; Hou, L.; Wei, Y. Facile Synthesis of Hierarchical Mesoporous Honeycomb-like NiO for Aqueous Asymmetric Supercapacitors. *ACS Appl. Mater. Interfaces* **2015**, *7*, 19930–19940.

35 Li, X.; Jiang, L.; Zhou, C.; Liu, J.; Zeng, H. Integrating Large Specific Surface Area

and High Conductivity in Hydrogenated $NiCo_2O_4$ Double-Shell Hollow Spheres to Improve Supercapacitors. *NPG Asia Mater.* **2015**, *7*, e165.

36 Cheng, D.; Yang, Y.; Xie, J.; Fang, C.; Zhang, G.; Xiong, J. Hierarchical $NiCo_2O_4$@$NiMoO_4$ Core–shell Hybrid Nanowire/nanosheet Arrays for High-Performance Pseudocapacitors. *J. Mater. Chem. A* **2015**, *3*, 14348–14357.

37 Wang, X.; Liu, W. S.; Lu, X.; Lee, P. S. Dodecyl Sulfate-Induced Fast Faradic Process in Nickel Cobalt Oxide–reduced Graphite Oxide Composite Material and Its Application for Asymmetric Supercapacitor Device. *J. Mater. Chem.* **2012**, *22*, 23114–23119.

38 Yang, J.; Li, G.; Pan, Z.; Liu, M.; Hou, Y.; Xu, Y.; Deng, H.; Sheng, L.; Zhao, X.; Qiu, Y.; Zhang, Y. All-Solid-State High-Energy Asymmetric Supercapacitors Enabled by Three-Dimensional Mixed-Valent MnO_x Nanospike and Graphene Electrodes. *ACS Appl. Mater. Interfaces* **2015**, *7*, 22172−22180.

39 Senthilkumar, B.; Meyrick, D.; Lee, Y.-S.; Selvan, R. Synthesis and Improved Electrochemical Performances of Nano β-$NiMoO_4$–$CoMoO_4 \cdot xH_2O$ Composites for Asymmetric Supercapacitors. *RSC Adv.* **2013**, *3*, 16542–16548.

40 Ma, X.-J.; Kong, L.-B.; Zhang, W.-B.; Liu, M.-C.; Luo, Y.-C.; Kang, L. Design and Synthesis of 3D Co_3O_4@$MMoO_4$ (M=Ni, Co) Nanocomposites as High-Performance Supercapacitor Electrodes. *Electrochim. Acta* **2014**, *130*, 660–669.

41 Xiao, K.; Xia, L.; Liu, G.; Wang, S.; Ding, L.-X.; Wang, H. Honeycomb-like $NiMoO_4$ Ultrathin Nanosheet Arrays for High-Performance Electrochemical Energy Storage. *J. Mater. Chem. A* **2015**, *3*, 6128-6135.

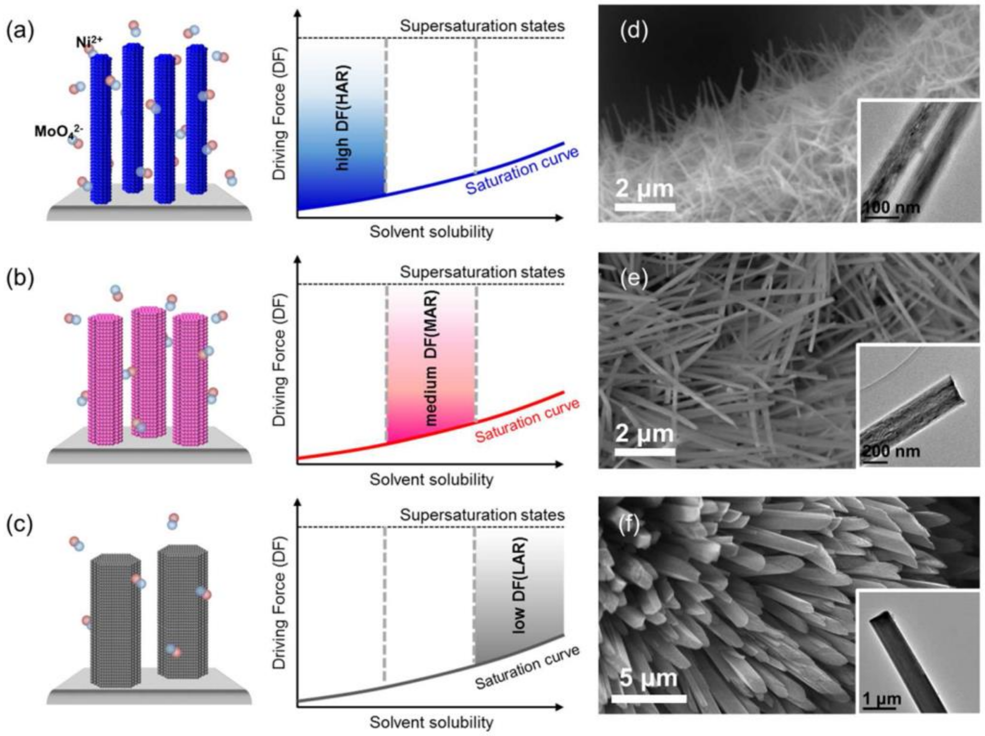

Figure 1. Hong *et. al.*

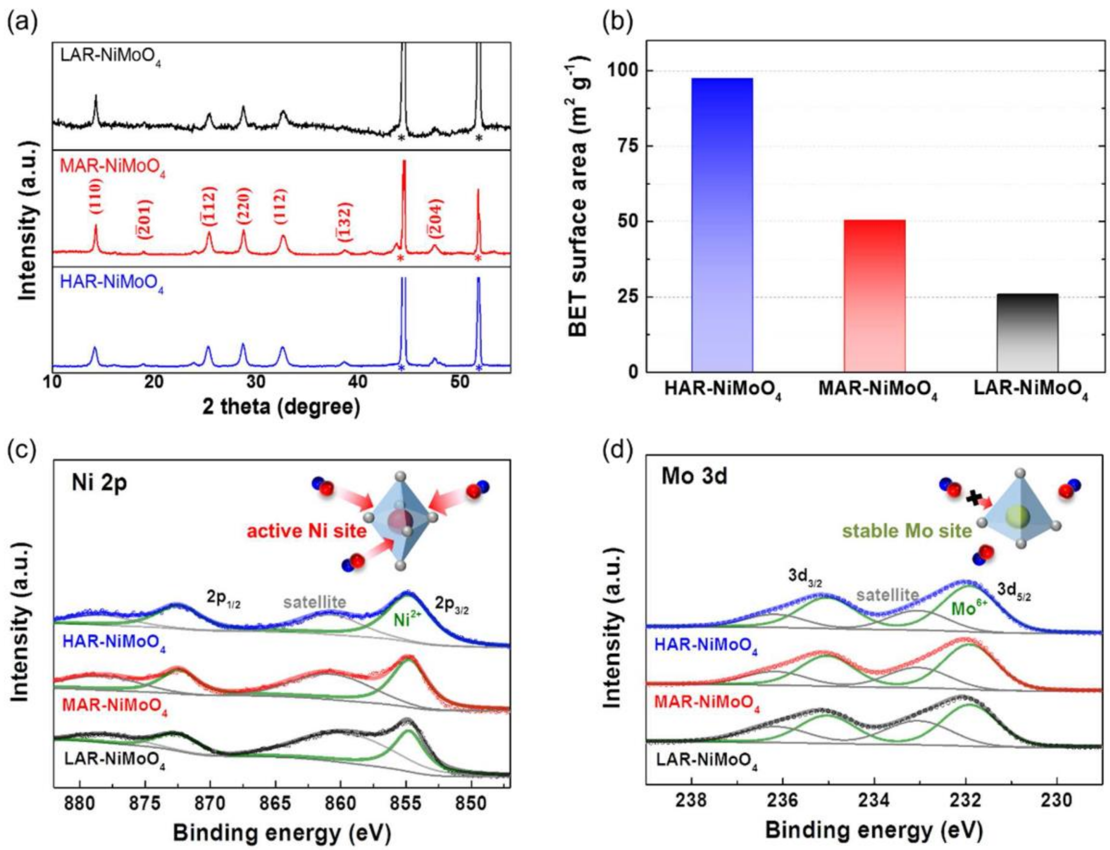

Figure 2. Hong *et. al.*

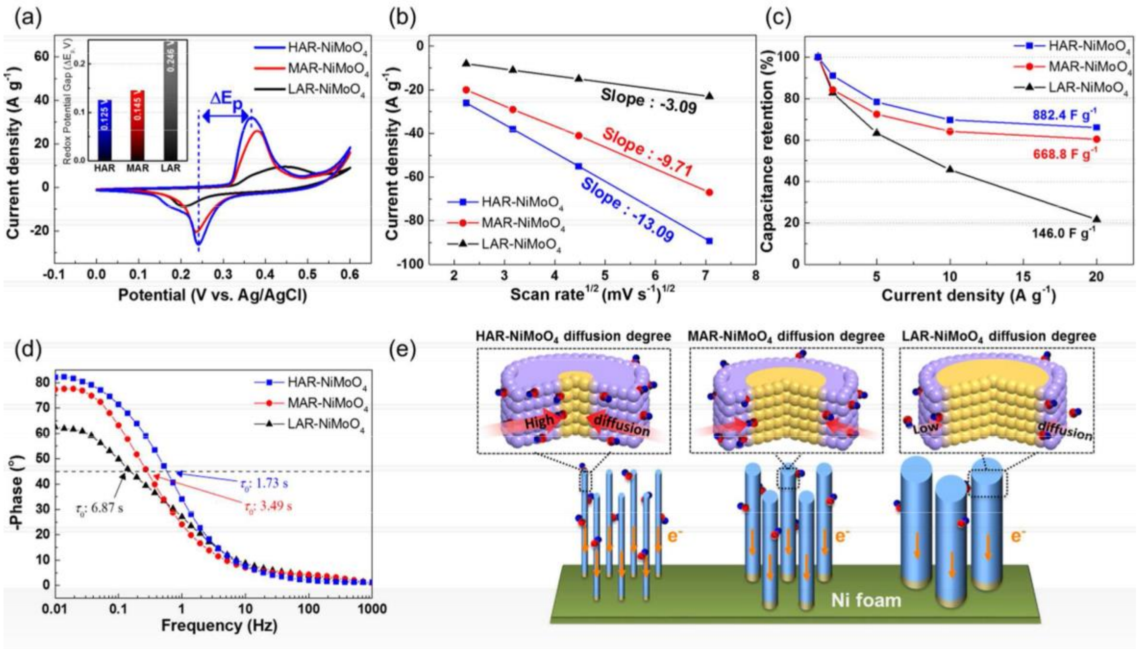

Figure 3. Hong *et. al.*

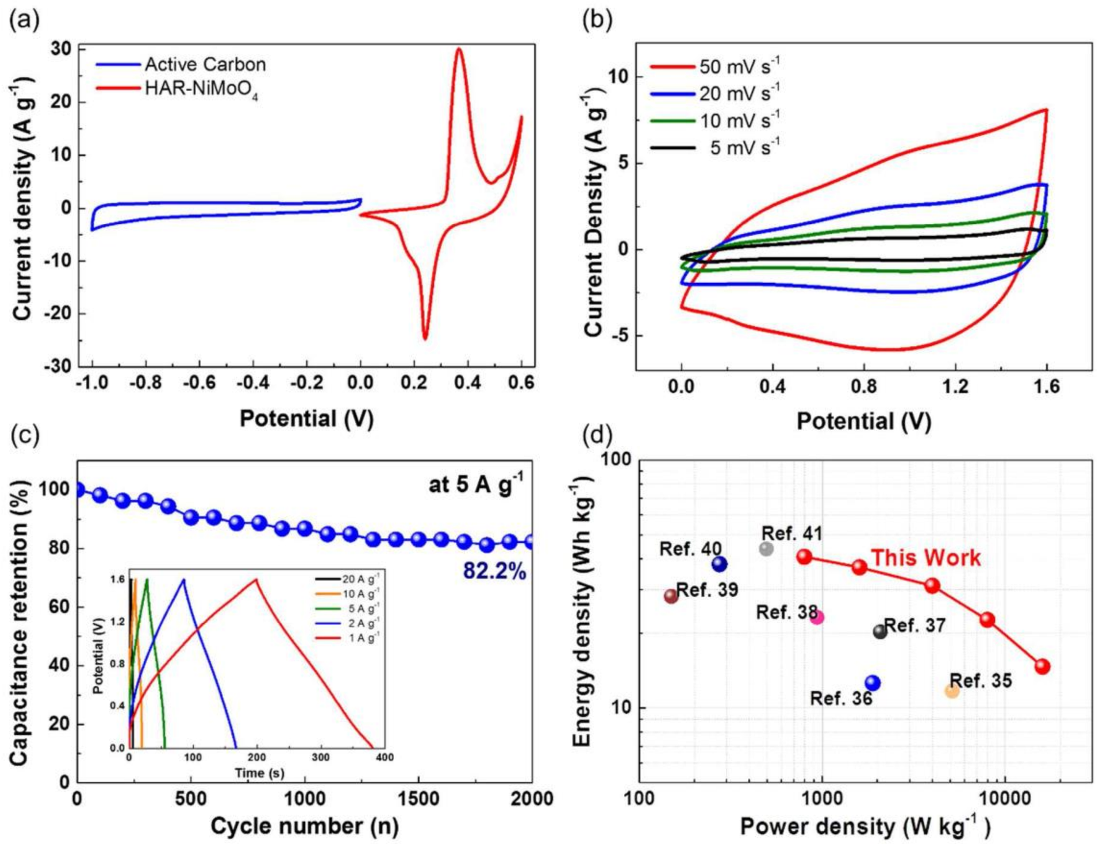

Figure 4. J. Hong *et. al.*

Table of Contents